Id4 modulates salivary gland homeostasis and its expression is downregulated in IgG4-related disease via miR-486-5p

木村, 宗惟

出版情報：九州大学, 2022, 博士（歯学）, 課程博士
バージョン：

BBA - Molecular Cell Research 1870 (2023) 119404

Contents lists available at ScienceDirect

BBA - Molecular Cell Research

journal homepage: www.elsevier.com/locate/bbamcr

Research paper

Id4 modulates salivary gland homeostasis and its expression is downregulated in IgG4-related disease *via* miR-486-5p

Yoshikazu Hayashi [a,b], Soi Kimura [a,c], Ena Yano [a], Shohei Yoshimoto [d,e], Ayaka Saeki [a], Atsushi Yasukochi [c], Yuji Hatakeyama [b], Masafumi Moriyama [a,c], Seiji Nakamura [c], Eijiro Jimi [a], Tomoyo Kawakubo-Yasukochi [a,*]

[a] OBT Research Center, Faculty of Dental Science, Kyushu University, 3-1-1 Maidashi, Higashi-ku, Fukuoka 812-8582, Japan
[b] Division of Functional Structure, Department of Morphological Biology, Fukuoka Dental College, 2-15-1 Tamura, Sawara-ku, Fukuoka 814-0193, Japan
[c] Section of Oral and Maxillofacial Oncology, Division of Maxillofacial Diagnostic and Surgical Sciences, Faculty of Dental Sciences, Kyushu University, 3-1-1 Maidashi, Higashi-ku, Fukuoka 812-8582, Japan
[d] Section of Pathology, Department of Morphological Biology, Division of Biomedical Sciences, Fukuoka Dental College, Fukuoka 814-0193, Japan
[e] Oral Medicine Research Center, Fukuoka Dental College, Fukuoka 814-0193, Japan

ARTICLE INFO

Keywords:
Id4
miR-486-5p
Salivary glands
Differentiation
Th17
IgG4-RD

ABSTRACT

Salivary glands are physiologically orchestrated by the coordinated balance between cell differentiation, proliferation, apoptosis, and interactions between epithelial, mesenchymal endothelial, and neuronal cells, and they are frequent sites of manifestations of Sjögren's syndrome (SS) or IgG4-related disease (IgG4-RD). However, little is known about salivary gland homeostasis and its involvement in those diseases. Inhibitor of DNA binding/differentiation 4 (Id4) is an Id protein involved in the transcriptional control of many biological events, including differentiation. Studies of Id4-deficient mice revealed that Id4-deficient submandibular glands were smaller and exhibited accelerated differentiation, compared with those from wild-type littermates. In addition, dry mouth symptoms and Th17 expansion in splenocytes were also observed in the absence of Id4. Furthermore, Id4 levels in the salivary glands of patients with IgG4-RD, but not SS, were significantly decreased compared with those of healthy controls. miRNA-mRNA integrated analysis demonstrated that miR-486-5p was upregulated in IgG4-RD patients and that it might regulate Id4 in the lesion sites. Together, these results provide evidence for the inhibitory role of Id4 in salivary differentiation, and a critical association between Id4 downregulation and IgG4-RD.

1. Introduction

The inhibitors of DNA binding/differentiation (ID/Id) protein family, comprising Id1, Id2, Id3, and Id4, are dominant negative transcriptional regulators of basic helix-loop-helix (bHLH) transcription factors that lack a DNA-binding domain [1]. Id proteins have critical roles in cell proliferation and differentiation [2,3], and the deletion of each Id protein demonstrated its involvement in various physiological and pathological conditions [4]. Among them, the expression patterns or functions of Id4 are thought to be distinct from those of Id1, Id2, and Id3 [5–7], and little is known about the role of Id4 in physiological and pathological processes.

Previous reports demonstrated that Id4 regulated mammary grand development by antagonizing HEB, a bHLH transcription factor [8,9], and that Id4 deficiency attenuated osteoblast differentiation from mesenchymal stem cells (MSCs) [10]. MSCs are a heterogenous population of stem cells that can be derived from multiple tissues, including salivary glands [11]; therefore, these findings prompted us to investigate

Abbreviations: Id4, inhibitor of DNA binding/differentiation 4; IgG4-RD, IgG4-related disease; SS, Sjögren's syndrome; SMGs, submandibular glands; ID/Id, inhibitors of DNA binding/differentiation; MSCs, mesenchymal stem cells; *Id4*$^{-/-}$, Id4-deficient; IL, interleukin; miRNA, microRNA; RSMG-1, rat normal salivary gland cell line; *Id4*$^{+/+}$, wild-type; SPF, specific pathogen-free; LGs, labial glands; HE, hematoxylin and eosin; PAS, Periodic Acid-Schiff; PCNA, proliferating cell nuclear antigen; PBMCs, peripheral blood mononuclear cells; P21, postnatal day 21; PI, propidium iodide; 7-AAD, 7-amino-actinomycin D; SE, standard error of the mean; Th, T helper.

* Corresponding author.
E-mail address: tomoyo@dent.kyushu-u.ac.jp (T. Kawakubo-Yasukochi).

https://doi.org/10.1016/j.bbamcr.2022.119404
Received 26 July 2022; Received in revised form 9 November 2022; Accepted 23 November 2022
Available online 17 December 2022

whether Id4 is involved in the differentiation of salivary glands and salivary pathological conditions.

In this study, we used Id4-deficient (*Id4*$^{-/-}$) mice and human serum and salivary glands from patients of Sjögren's syndrome (SS) and IgG4-related disease (IgG4-RD), in which salivary glands are a frequent location of lesions. IgG4-RD patients develop an immune-mediated and chronic fibroinflammatory condition with high serum IgG4 concentrations, which are used as a traditional biomarker for IgG4-RD [12]. In addition, IgG2, interleukin (IL)-2 receptor, and CC-chemokine ligand 18 were suggested to be new biomarkers for IgG4-RD because of their close relationship with inflammation and fibrosis [13]. However, currently, there is no definitive biomarker for IgG4-RD except for elevated serum IgG4 levels and IgG4-positive plasma cell infiltration into the affected tissues. This disease is often compared to SS because of their clinical similarities, but there are many differences in clinical, serological, and histopathological characteristics between IgG4-RD and SS, and therefore they are defined as completely different diseases [14]. To elucidate the etiology and pathology of IgG4-RD, various approaches with an immunological focus have been attempted [15]. Among these, Nezu et al. recently examined the expression profiles of microRNAs (miRNAs) in IgG4-related ophthalmic disease, and have reported that it differs dynamically compared with healthy controls [16]. miRNAs are small non-coding RNAs that function as a guide in RNA silencing, *via* the cleavage and degradation of the target mRNA or translational repression, and these events eventually regulate various biological systems [17,18].

Here, we identified Id4 as an important regulator of salivary gland differentiation and physiological immune balance, and its deficiency caused pathology similar to IgG4-RD. In addition, miRNA-mRNA integrated analysis using human samples revealed that Id4 might be downregulated by hsa-miR-486-5p in IgG4-RD salivary glands. These new roles of Id4 in salivary gland homeostasis and the immune system of mammals will help identify new biomarkers, such as hsa-miR-486-5p and Id4, for use in clinical practice to diagnose IgG4-RD.

2. Material and methods

2.1. Cells

A rat normal salivary gland cell line (RSMG-1), purchased from JCRB Cell Bank (Osaka, Japan), was maintained as described previously [19]. In brief, the cells were cultured on culture dishes coated with type I collagen (Cell matrix Type IA, Nitta Gelatin, Osaka, Japan) in MCDB153 medium (Sigma-Aldrich, St. Louis, MO) containing 0.11 g/l sodium pyruvate (Nacalai Tesque, Kyoto, Japan), 100 mg/l isoleucine (Fujifilm Wako, Osaka, Japan), and 1.18 g/l sodium hydrogen carbonate (Fujifilm Wako). Culture medium was supplemented with 10 μg/ml bovine insulin (Sigma-Aldrich), 5 μg/ml human transferrin (Sigma-Aldrich), 10 μM 2-mercaptoethanol (Nacalai Tesque), 10 μM 22-aminoethanol (Sigma-Aldrich), and 1 ng/ml recombinant rat FGF-1 (PeproTech, Rocky Hill, NJ). Human adenocarcinoma cell lines, PC-3 (prostate), MCF7 (breast), and Caco-2 (colon), were purchased from RIKEN Bio-Resource Research Center (Tsukuba, Japan) and cultured in DMEM (Fujifilm Wako) supplemented with 10 % fetal bovine serum (Thermo Fisher Scientific, Waltham, MA). All cells were maintained in a humidified atmosphere of 5 % CO_2 at 37 °C.

2.2. Mice

Id4$^{-/-}$ mice previously generated at the University of Nottingham (Nottingham, UK) [20] were available from Riken BRC (RBRC04832). *Id4*$^{-/-}$ mice and their wild-type (*Id4*$^{+/+}$) littermates were maintained in a specific pathogen-free (SPF) facility under a 12/12 h light/dark cycle with food and water provided *ad libitum*. All mice used in this study were maintained and handled in accordance with the protocols approved by the animal ethics committee of Kyushu University (permission no. A20-261 and A22-055).

2.3. Pilocarpine-stimulated saliva secretion test

After mice were anesthetized with medetomidine, midazolam, and butorphanol, a preweighed cotton ball was placed in their mouths sublingually, and 5 μg/g body weight of pilocarpine (#28008-31, Nacalai Tesque) was injected intraperitoneally to stimulate saliva secretion. The cotton ball was changed every 10 min for 30 min, and the amount of secreted saliva was calculated using the collected cotton balls.

2.4. SMG organ culture

SMGs at embryonic day 13.5 (E13.5) from timed-pregnant female mice were dissected as described previously [21]. SMGs were cultured on Nunc Polycarbonate Cell Culture Inserts (0.4 μm pore size, #140620, Thermo Fisher Scientific, Waltham, MA) and the filters were floated on 300 μl of DMEM/F12 medium (#05177-15, Nacalai Tesque) with 100 U/ml penicillin, 100 μg/ml streptomycin, 100× Glutamax (#35050-061, Gibco), 100× N-2 Supplement (#17502-048 Gibco), 100× Insulin-Transferrin Selenium (ITS-G) (#41400-045, Gibco), 50 nM Hydrocortisone (18403-51, Nacalai Tesque), 10 U/ml Heparin (17513–96, Nacalai Tesque), 50 ng/ml recombinant human FGF-2 (100-18B, PeproTech), 100 ng/ml recombinant human FGF-7 (100-19, PeproTech), and 100 ng/ml recombinant human FGF-10 (100-26, PeproTech). SMGs in the *Id4*$^{+/-}$ and *Id4*$^{+/+}$ were cultured on each filter in a humidified atmosphere of 5 % CO_2 at 37 °C. Photomicrographs of SMGs were captured using a microscopy photographed after SMG dissection (Day 0), 24 h (Day 1), 48 h (Day 2), 72 h (Day 3), and 96 h (Day 4).

2.5. Human samples

This study was approved by the Ethics Committee of Kyushu University, Japan, and written informed consent was obtained from all participants (IRB serial numbers: 25-287 and 834-01). Human samples of serum and salivary glands (SMGs or labial glands (LGs)) were obtained from 17 IgG4-RD patients (nine male and eight female; mean [±SD] age, 62.6 ± 10.7 years), five primary Sjögren's syndrome (SS) patients (five female; mean [±SD] age, 60.0 ± 16.1 years), and five mucocele patients as healthy controls (five female; mean [±SD] age, 39.4 ± 14.4 years). SMG from healthy donors (male, 23 years) and serum samples (n = 4, two male and two female donors; mean [±SD] age, 64.8 ± 12.7 years) obtained with informed consent in accordance with the Declaration of Helsinki were purchased from BioChain Institute Inc. (Newark, CA) and Kohjin Bio (Saitama, Japan), respectively.

2.6. Immunohistochemical analysis

Tissue samples were embedded in paraffin, subjected to hematoxylin and eosin (HE) staining, Periodic Acid-Schiff (PAS) staining, or immunohistochemistry (performed by Morphotechnology Co. Ltd. (Hokkaido, Japan) and Biopathology Institute Co., Ltd. (Oita, Japan)), using primary antibodies for Id4 (1:80, Abgent, San Diego, CA), AQP5 (dilution 1:6000, #178615, Sigma), CK14 (dilution 1:1000, ab181595, Abcam), α-SMA (dilution 1:300, M0851, Daco), proliferating cell nuclear antigen (PCNA) (dilution 1:1000, #2586, Cell Signaling), and COL17A (dilution 1:1000, ab184996, Abcam), incubated for 1 h at room temperature and CK19 (dilution 1:500, ab133496, Abcam) overnight at 4 °C based on the polymers method. For quantification of Id4 staining, Id4 stained area in nuclei of acinar cell was automatically counted using a hybrid cell count application (BZ-H4C, Keyence, Osaka, Japan) in the BZ-X800 Analyzer software BZ-H4A (Keyence), and calculated the ratios as follows: positive nuclei area/ total area of acinar cells. For immunofluorescence staining, serum from *Id4*$^{+/+}$ and *Id4*$^{-/-}$ mice at postnatal day 21 (P21) and Alexa Fluor 568-conjugated goat anti-mouse IgG (#A11004, Thermo Fisher Scientific, Waltham, MA) were used as the primary and

secondary antibodies, respectively. Sections were mounted using VECTASHIELD with DAPI (#H-1800, Vector Lab., Burlingame, CA). Photomicrographs were visualized and captured at the appropriate wavelength using a fluorescence microscope (LSM 710, Carl Zeiss Inc.). The images were processed using ZEN 2010B Sp1 Ver. 6.0.0.485 software (Carl Zeiss Inc.).

2.7. RNA in situ hybridization for tissues

Neutral buffered formalin (10 %)-fixed and paraffin-embedded tissue blocks were cut into 4 μm-thick sections for RNA *in situ* hybridization. To detect *Id4* mRNA, the *in situ* hybridization system RNAscope® (Advanced Cell Diagnostics, Hayward, CA, USA) was used following the manufacturer's guidelines. Photomicrographs were captured using a microscopy and *Id4* positive signals were quantified using ImageJ.

2.8. Microarray analysis (miRNA-mRNA integrated analysis)

Total RNA was isolated from serum using Sepasol-RNA I Super G (Nacalai Tesque). RNA samples were quantified with an ND-1000 spectrophotometer (NanoDrop, Wilmington, DE) and the quality was confirmed with an Experion System (Bio-Rad, Hercules, CA). Total RNA (100 ng) in each sample was labeled using a FlashTag™ Biotin HSR RNA Labeling Kit and hybridized to an Affymetrix GeneChip miRNA 4.0 Array following the manufacturer's instructions. All hybridized microarrays were scanned with an Affymetrix scanner. Relative hybridization intensities and background hybridization values were calculated using Affymetrix Expression Console™. The raw CEL files for gene-level analyses were processed with median polish summarization and quantile normalization in Affymetrix® Transcriptome Analysis Console Software to obtain normalized intensity values. We calculated the ratios to identify up- or downregulated genes (non-log scaled fold-change ratios were calculated from the healthy and IgG4-RD groups and intensities normalized to identify upregulated ($\geq$2.0-fold) or downregulated ($\leq$0.5-fold) genes). After the treatment of RSMG-1 cell cultures with serum from IgG4-RD patients or healthy donors for 24 h, total RNA was isolated from RSMG-1 cells using Sepasol-RNA I Super G and purified with a High Pure RNA isolation kit (Roche) following the manufacturer's instructions. RNA samples were quantified with an ND-1000 spectrophotometer (NanoDrop) and quality was confirmed with an Experion System (Bio-Rad). The cRNA was amplified, labeled using a GeneChip® WT Terminal Labeling and Control Kit, and hybridized to Agilent SurePrintG3 Rat GE Microarray 8x60K following the manufacturer's instructions. To identify up- or downregulated genes, we calculated the Z-scores and non-log scaled fold-change ratios from the normalized signal intensities of each probe. The criteria for up- or downregulated genes were as follows: upregulated genes, Z-score $\geq$ 2.0 and ratio $\geq$ 1.5-fold; downregulated genes, Z-score $\leq$ −2.0 and ratio $\leq$ 0.66. Each related human miRNA was searched by miRNA target prediction resources from Affymetrix (Santa Clara, CA) mainly based on miRTarBase [22], microcosm [23], and TargetScan [24,25].

2.9. Quantitative PCR (qPCR) analysis

For mRNA RT-qPCR, total RNA was extracted from tissues using Sepasol-RNA I Super G (Nacalai Tesque) and a High Pure RNA Isolation Kit (Roche Diagnostics, Mannheim, Germany). The RNA was reverse transcribed using a Verso cDNA Synthesis Kit (Thermo Fisher Scientific), and the resulting cDNA was subjected to two-step qPCR analysis with a LightCycler 480 system (Roche Diagnostics) using the TaqMan method. The cycling conditions were as follows: 95 °C for 10 min (hot-start PCR), followed by 45 cycles of 95 °C for 15 s, 60 °C for 30 s, and 72 °C for 1 s. The PCR primer sequences (forward and reverse), TaqMan probes specific for each sequence (Roche Diagnostics), and amplicon sizes are described in Supplemental Table 1. For the SYBR green method, the cycling conditions were as follows: 95 °C for 10 min (hot-start PCR), followed by 40 cycles of 95 °C for 5 s and 60 °C for 30 s, using the PowerUp SYBR Green Master Mix (Applied Biosystems, Waltham, MA) and StepOne Plus Real-Time PCR system (Applied Biosystems). The PCR primer sequences and amplicon sizes are listed in Supplemental Table 2.

For miRNA RT-qPCR, miRNA extraction and qPCR were performed by using miRNA Isolation Kit (Roche Diagnostics), *Escherichia coli* poly (A) polymerase (New England Biolabs, Ipswich, MA, USA), miRNA EasyScript cDNA synthesis kit (Applied Biological Materials, Richmond, BC, Canada) and EvaGreen miRNA qPCR MasterMix (Applied Biological Materials). Primers for miR-486-5p and SNORD44 were purchased from Applied Biological Materials. The cycling conditions were as follows: 95 °C for 10 min, followed by 45 cycles of 95 °C for 10 s, 63 °C for 15 s and 72 °C for 5 s. A melting curve analysis (60 °C–99 °C) was performed after obtaining the thermal profile to ensure specificity in the amplification.

2.10. miRNA mimic and inhibitor transfection

miRNA mimics and inhibitors and each control were purchased from Bioneer (Daejeon, Korea) and transfected with GeneSilencer transfection reagent (Genlantis, San Diego, CA).

2.11. Immunoblot analysis

Cells or tissues were lysed and homogenized in RIPA buffer (Fujifilm Wako) containing a protease inhibitor cocktail (Nacalai Tesque). After centrifugation, the supernatants were collected and the protein concentrations of the samples were measured using a BCA Protein assay kit (Fujifilm Wako). Each sample (25 μg/tube) was supplemented with SDS-PAGE sample buffer containing 2-mercaptoethanol (Nacalai Tesque), incubated at 95 °C for 5 min, and then separated by glycine-based 5 %–20 % gradient SuperSep precast gels (Fujifilm Wako). The separated proteins were then transferred onto Immobilon PVDF membranes (Merck Millipore) and non-specific protein binding was blocked using Blocking One (Nacalai Tesque) for 1 h at room temperature. The following primary antibodies were used: anti-Id4 (dilution 1:1000, sc-365656, Santa Cruz Biotechnology), anti-AQP5 (dilution 1:4000, 178,615, Calbiochem, Temecula, CA), anti-CK14 (dilution 1:20,000, #905304, BioLegend, San Diego, CA), anti-CK19 (dilution 1:4000, ab133496, Abcam), anti-PCNA (dilution 1:4000, #2586, Cell Signaling Technology, Danvers, MA), anti-SEL-1L (dilution 1:1000, sc-377,351, Santa Cruz Biotechnology), anti-GAPDH (dilution 1:40,000, # 60004-1-lg, Proteintech), and anti-Actin (dilution 1:40,000, # M177-3, MBL) at 4 °C overnight. After incubation with a primary antibody, the membranes were washed with Tris-buffered saline containing 0.1 % Tween-20 (Fujifilm Wako) and incubated at 4 °C overnight with the appropriate secondary antibodies coupled to HRP: anti-rabbit (dilution 1:5000, Cell Signaling Technology, Danvers, MA) for Id4, SEL-1L, and AQP5, and anti-mouse (dilution 1:40,000, Cell Signaling Technology) for GAPDH and actin. After washing, the membranes were analyzed using the ImageQuant LAS4000 system (GE Healthcare, Chicago, IL) after incubation with Amersham ECL reagent (Cytiva, Tokyo, Japan).

2.12. Flow cytometry

Cells from the spleen and peripheral blood mononuclear cells (PBMCs) were pre-incubated for 10 min at RT with purified anti-CD16/32 antibody (dilution 1:100, #101301, BioLegend) to block the FcγR, followed by staining with antibodies purchased from BioLegend: anti-B220 (dilution 1:100, #103205), anti-CD3ε (dilution 1:100, #100305), anti-CD4 (dilution 1:1100, #100413), anti-CD8a (dilution 1:100, #100733), anti-CXCR3 (dilution 1:100, #126541), anti-CCR4 (dilution 1:100, #131211), and anti-CCR6 (dilution 1:100, #129803) and incubated for 1 h at 4 °C. The labeled cells were then washed and analyzed with FACSVerse (BD Biosciences, Franklin Lakes, NJ). Dead cells were eliminated by labeling cells with propidium iodide (PI)

(concentration 2 μg/ml, #19174-31, Nacalai Tesque) or 7-amino-actinomycin D (7-AAD) (concentration 0.25 μg/ml, #559925, BD Biosciences). Subsequent analysis of flow cytometry data was performed using FlowJo software (version 10.6.1, BD Biosciences).

2.13. Statistical analysis

Student's *t*-test (two-tailed *t*-test), Welch's *t*-test (two-tailed *t*-test), multiple unpaired *t*-test, ANOVA followed by Dunnett's test or Tukey-Kramer test, and Kruskal Wallis test followed by Dunn's multiple comparison test were performed as appropriate using JMP software (ver. 14; Cary, NC, USA) and GraphPad Prism 9 software (version 9.4.0, Graph pad software, San Diego, CA). All quantitative data are indicated as the mean ± standard error of the mean (SE) unless otherwise indicated. *P* values < 0.05 were considered statistically significant.

3. Results

3.1. Body size and mortality of Id4-deficient ($Id4^{-/-}$) mice

As reported previously [20], $Id4^{-/-}$ mice died at an early age, approximately 3 weeks of age (3-wks) under SPF conditions. Of note,

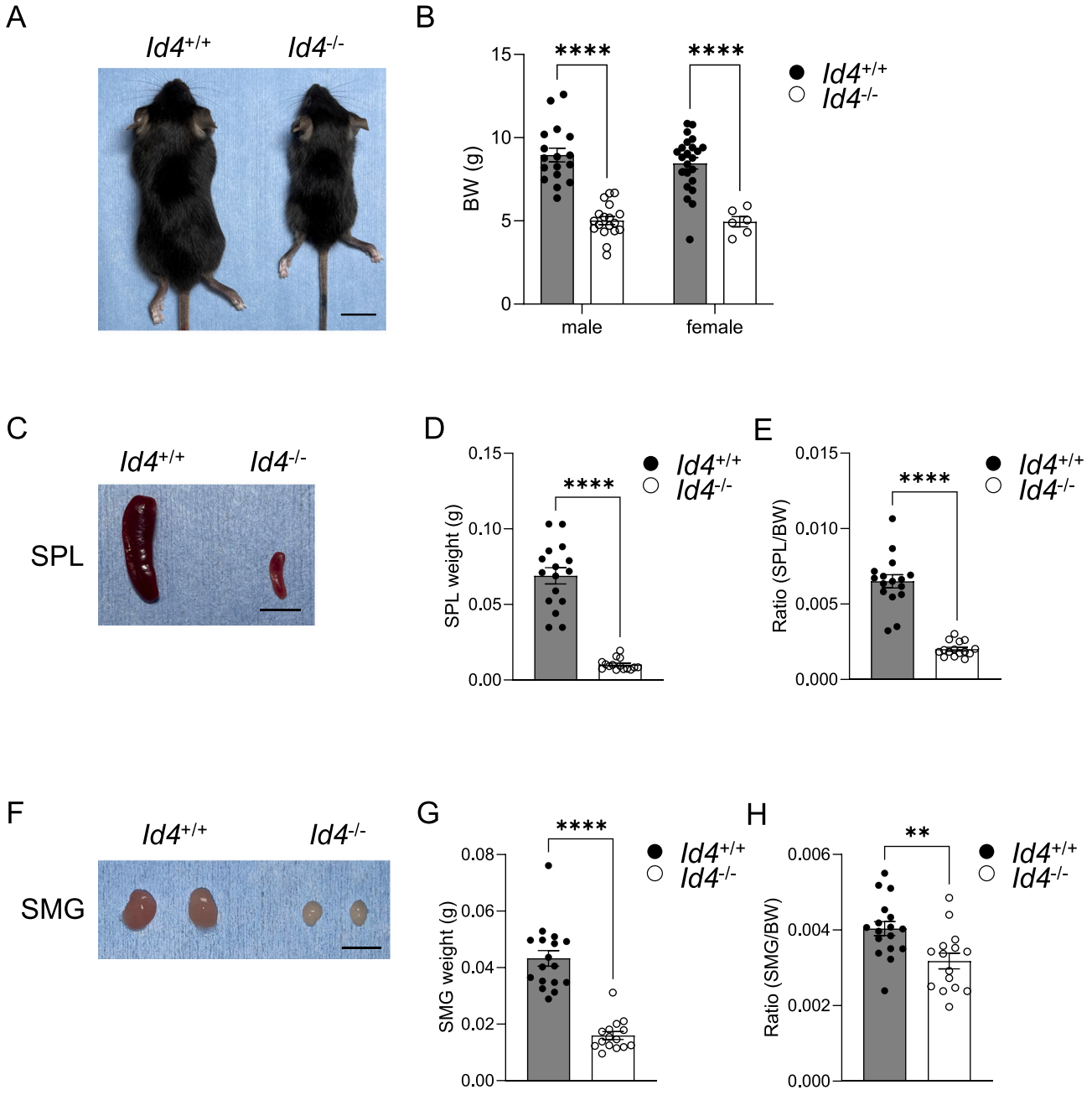

Fig. 1. $Id4^{-/-}$ mice show organ and body weight loss.
(A) Representative images of $Id4^{+/+}$ and $Id4^{-/-}$ mice at P21. Scale bars: 10 mm. (B) Body weight at P21 ($Id4^{+/+}$, $n = 17$ male and $n = 23$ female; $Id4^{-/-}$, $n = 18$ male and $n = 6$ female). Few female $Id4^{-/-}$ mice lived to P21. (C) Representative images of spleens (SPL) from $Id4^{+/+}$ and $Id4^{-/-}$ mice at P21. Scale bars: 5 mm. (D–E) The weight of the SPL (D) and its weight ratio to the body weight (E) at 3-wks ($Id4^{+/+}$ $n = 16$; $Id4^{-/-}$ $n = 15$). (F) Representative images of the SMG in $Id4^{+/+}$ and $Id4^{-/-}$ mice at P21. Scale bars: 5 mm. (G–H) The weight of the SMG (G) and its weight ratio to the body weight (H) at 3-wks ($Id4^{+/+}$ n = 17; $Id4^{-/-}$ n = 15). Data are expressed as the mean ± SE from three independent experiments. Multiple unpaired *t*-test and Student's *t*-test (two-tailed) were used. $^{**}P < 0.01$, $^{****}P < 0.0001$.

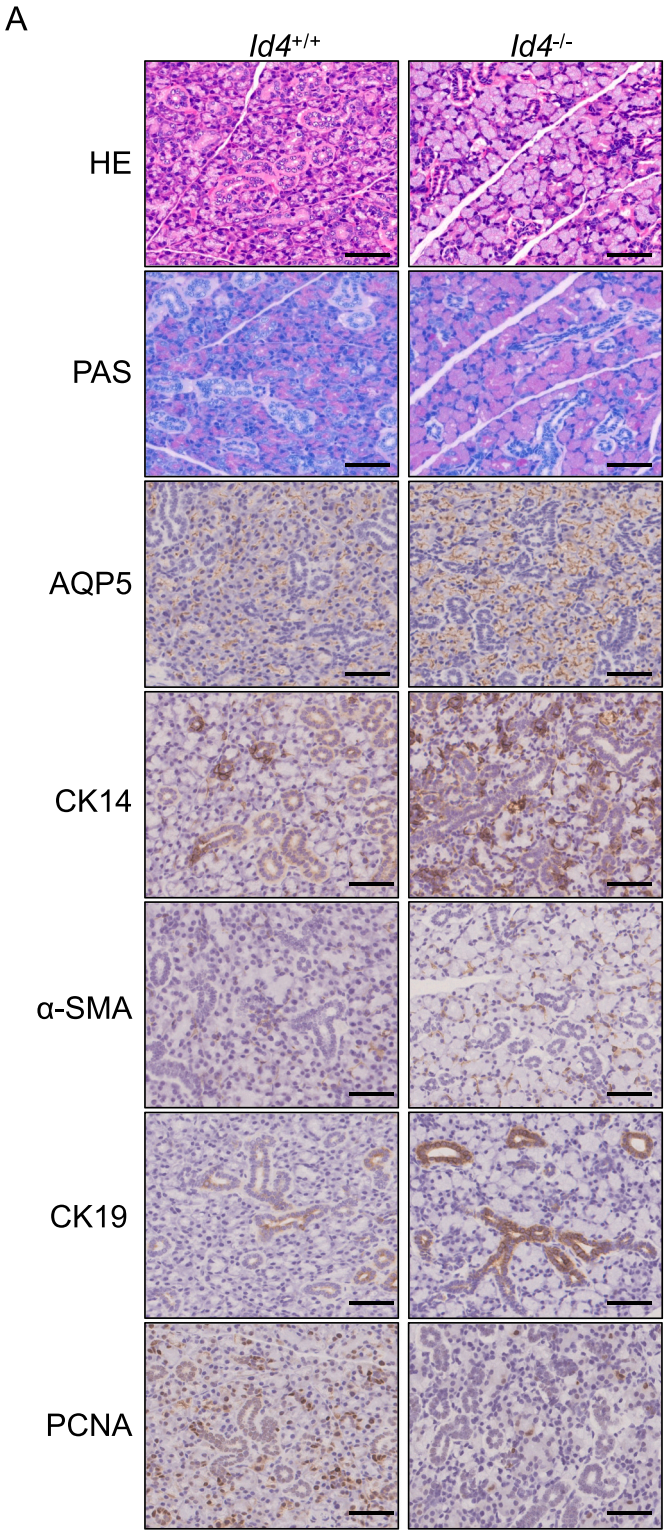

Fig. 2. Id4 deficiency induces morphological and functional abnormalities in mouse SMG.
(A) Hematoxylin and eosin (HE), PAS, and immunohistochemical staining for AQP5, CK14, α-SMA, CK19, and PCNA in the SMG of $Id4^{+/+}$ ($n = 3$–5) and $Id4^{-/-}$ mice (n = 3–6) at P21. Scale bars: 50 μm. Representative data are shown. (B) Representative images of immunoblot bands for Id4, AQP5, CK14, CK19, PCNA, and β-actin (used as a loading control) in the SMG from $Id4^{+/+}$ ($n = 5$) and $Id4^{-/-}$ (n = 5) mice at P21. (C) Each panel represents densitometrical band quantification from (B). A two-tailed Student's *t*-test was used. $^{*}P < 0.05$, $^{**}P < 0.01$, $^{***}P < 0.001$. (D) Saliva secretion test of $Id4^{+/+}$ and $Id4^{-/-}$ mice ($Id4^{+/+}$ $n = 8$; $Id4^{-/-}$ n = 5). Saliva weight was normalized to the body weight of each animal. (E) Immunofluorescent detection of autoantibodies against the SMG tissues. Serum from $Id4^{+/+}$ and $Id4^{-/-}$ mice at P21 and Alexa Fluor 568-conjugated goat anti-mouse IgG were used as the primary and secondary antibodies, respectively. Young or aged SMG were dissected from P21 or 24-week-old female $Id4^{+/+}$ mice. Scale bars: 50 μm. All experiments were repeated three times independently, and representative results are shown. A two-tailed Student's *t*-test was used. $^{***}P < 0.001$.

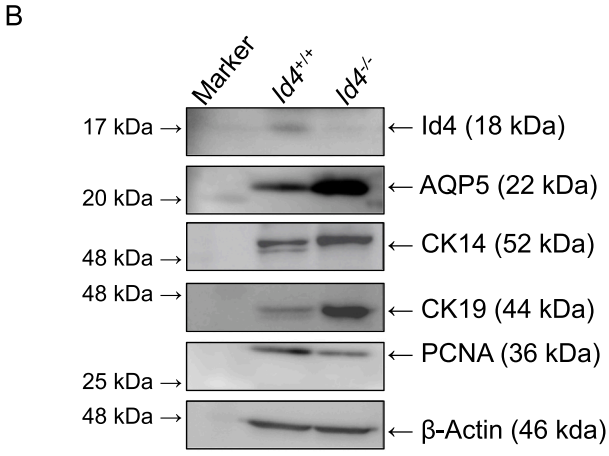

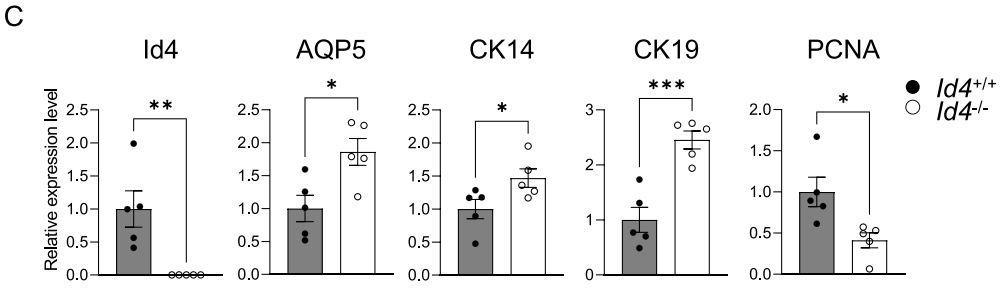

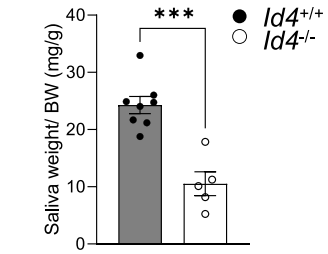

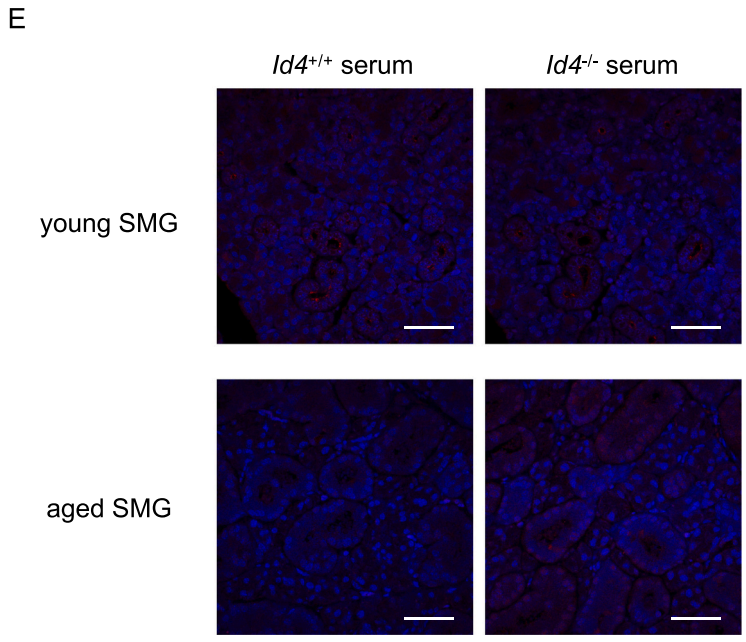

Fig. 2. (*continued*).

some female *Id4*$^{-/-}$ mice survived up to P21. The body size and weight of *Id4*$^{-/-}$ mice were significantly decreased, with approximately 40 % weight loss occurring at P21 compared with *Id4*$^{+/+}$ littermates (Fig. 1A, B). This body weight loss caused by *Id4* deficiency was also associated with a decrease in the size of various organs, including the spleen (Fig. 1C, D) and SMGs (Fig. 1F, G). Moreover, the absolute weight of each organ (Fig. 1D, G) and the ratio of each organ to the body weight (Fig, 1E, H) were significantly reduced in *Id4*$^{-/-}$ mice compared with *Id4*$^{+/+}$ mice. These results suggest that functional or structural abnormalities are present in the spleen and SMG of *Id4*$^{-/-}$ mice.

3.2. SMG in *Id4*$^{-/-}$ mice have abnormal morphogenesis and functional disorders

To confirm the effect of Id4 on SMG development, we observed branching morphogenesis of SMG from *Id4*$^{+/+}$ and *Id4*$^{+/-}$ mice starting at embryonic day 13.5 (E13.5) by using organ cultures *exo vivo*, since SMG from *Id4*$^{-/-}$ mice at E13.5 showed below the limit of detection even under a microscope (data not shown). *Id4* gene expression level of SMGs in the *Id4*$^{+/-}$ mice was decreased by half compared to the SMG of *Id4*$^{+/+}$ (Fig. S1A), and SMG branching morphogenesis was decreased in the *Id4*$^{+/-}$ SMG between Day 0 and Day 4 compared to *Id4*$^{+/+}$ SMG (Fig. S1B). This result obviously indicates that Id4 directly affected morphological development in SMG (Fig. S1A, B). In addition, we also used an Activin A-induced cell differentiation model [26] with a rat normal salivary gland cell line, RSMG-1. RSMG-1 cells treated with Activin A for 24 h increased the expression level of Id4, as well as the acinar markers, SEL-1L [26] and AQP5 (Fig. S1C). Taken together, these results suggest that Id4 might be an important factor for normal differentiation in salivary glands.

Subsequently, we performed histological analysis to examine the expression patterns of differentiation markers in the SMG of *Id4*$^{-/-}$ mice at P21. Differentiation markers for salivary glands, including AQP5 (an acinar marker [27]), CK14 and α-SMA (myoepithelial markers [28]), and CK19 (ductal marker, [29]), were highly expressed in the SMG of *Id4*$^{-/-}$ mice compared with *Id4*$^{+/+}$ littermates (Fig. 2A). This tendency was confirmed by immunoblot analysis (Fig. 2B, C). In addition, we observed significant mucus accumulation in *Id4*$^{-/-}$ SMG by PAS staining analysis (Fig. 2A). These data suggest that Id4 deficiency might promote SMG differentiation. Although salivary glands generally contain a low percentage of proliferating cells and a higher degree of differentiating cells [30], the maintenance of tissue homeostasis is strictly regulated by a balance between cell proliferation and differentiation without exception in salivary glands [31]. Indeed, the expression level of PCNA, a marker of mitogenesis, was significantly decreased in *Id4*$^{-/-}$ SMG compared with *Id4*$^{+/+}$ SMG (Fig. 2A–C), supporting the altered balance between cell proliferation and differentiation in *Id4*$^{-/-}$ SMG.

Next, we examined the saliva secretion capacity of *Id4*$^{-/-}$ mice. Pilocarpine-stimulated saliva secretion in *Id4*$^{-/-}$ mice was significantly reduced by more than half compared with *Id4*$^{+/+}$ mice, even when considering the weight ratio, indicating *Id4*$^{-/-}$ mice developed dry mouth symptoms (Fig. 2D). Dry mouth, caused by the dysfunction of salivary glands, is associated with aging, radiation injury, drug side effects, inflammatory diseases, and abnormal tissue development [32,33]. In diseases of the maxillofacial area, salivary glands in SS and IgG4-RD typically undergo morphological and functional changes and are symptomatic of dry mouth to a greater or lesser extent [34]. In SS, the presence of autoantibodies such as anti-SS-A (SS-related antigen A) has been confirmed [35], although it is unknown whether the pathogenesis of IgG4-RD is related to an autoantibody. Therefore, we verified the presence or absence of autoantibodies in *Id4*$^{-/-}$ mice. Our immunofluorescence analysis, using serum from P21 *Id4*$^{+/+}$ or *Id4*$^{-/-}$ mice as a primary antibody, demonstrated no positive signal in SMG from young or aged *Id4*$^{+/+}$ mice (Fig. 2E), indicating the lack of autoantibodies against an SMG-related molecule in *Id4*$^{-/-}$ mice at least at 3-wks.

3.3. Id4 deficiency induces the expansion of Th17 cells in mice

To analyze the distribution of lymphocyte subpopulations in *Id4*$^{-/-}$ mice, we focused on the spleen, which is the largest secondary lymphoid organ. The size and weight of *Id4*$^{-/-}$ spleens and SMG were significantly decreased compared with those of *Id4*$^{+/+}$ littermates (Fig. 1C, D, E, F, G, H). Therefore, we clarified whether Id4 deficiency induced an immune disorder in mice. After confirming that Id4 protein was expressed in the spleens of *Id4*$^{+/+}$ mice (Fig. 3A), we performed a comparative analysis between *Id4*$^{-/-}$ and *Id4*$^{+/+}$ splenocytes using a flow cytometry-based method. Flow cytometry analysis showed that populations of CD3^{+}, CD4^{+}, and CD8^{+} T cells, but not B220^{+} B cells, were significantly increased in the spleens of *Id4*$^{-/-}$ mice compared with those of *Id4*$^{+/+}$ mice (Fig. 3B, C). These results suggest Id4 deficiency induced the generation of T cells rather than B cells. Subsequently, CD4^{+} T helper (Th) cell phenotypes in the spleens of *Id4*$^{-/-}$ mice were examined because they have central roles in immunity during physiological and pathological conditions [36]. As a result, a population of CD4^{+} CCR6^{+} T cells was markedly increased in the spleens of *Id4*$^{-/-}$ mice compared with *Id4*$^{+/+}$ mice (Fig. 3D, E, F). Although CCR6^{+} Th cells are heterogenous and contain several subpopulations [37], CCR6 is highly expressed by Th17 cells [37,38], and our quantitative ELISA data showed IL-17, a proinflammatory cytokine mainly produced by Th17 cells [39], was highly expressed in splenocytes from *Id4*$^{-/-}$ mice (Fig. 3G, H). Furthermore, the increased level of IL-17 was also observed in SMGs from *Id4*$^{-/-}$ mice (Fig. 3I). These results indicate *Id4*$^{-/-}$ mice had more prominent Th17 cell subset polarization, which was reported to be involved in several autoimmune and autoinflammatory pathologies [40]. We performed similar experiments using PBMCs. Our FACS data revealed that populations of CD3^{+}, CD4^{+}, and CD8^{+} T cells, but not B220^{+} B cells, were significantly increased in *Id4*$^{-/-}$ PBMCs compared with *Id4*$^{+/+}$ PBMCs (Fig. 3J, K). Additionally, the frequency of CD4^{+} cells was increased, whereas that of CD8^{+} was decreased in CD3^{+} T cells (Fig. 3L). In addition, the CD4/CD8 ratio was significantly greater in *Id4*$^{-/-}$ PBMCs than in *Id4*$^{+/+}$ PBMCs (Fig. 3M). Given that IL-17 secreting CD4^{+}CCR6^{+} Th17 cells are significantly increased in SS and IgG4-RD [41,42] and that the expansion of CD4^{+} T cells was observed in both diseases [43,44], our data suggest that *Id4*$^{-/-}$ mice develop similar immune balance to SS or IgG4-RD, in addition to salivary gland dysfunction (Fig. 2C).

3.4. Id4 expression is markedly reduced in the salivary glands of IgG4-RD patients

To investigate the involvement of Id4 expression in the pathogenesis of SS or IgG4-RD, histological analysis was performed using salivary glands from healthy donors, and SS and IgG4-RD patients. Id4 was highly expressed in the SMGs of healthy controls or LGs of the mucocele, which is usually used as a healthy control when investigating SS and IgG4-RD [45,46], in acinar and ductal cells, whereas its expression level was markedly decreased in those of IgG4-RD patients, but not in the LGs of SS patients (Fig. 4A). The quantitative evaluation of Id4-positive areas in each salivary gland showed that Id4 expression in the salivary glands of IgG4-RD patients was decreased by <25 % of that in healthy controls (Fig. 4B). However, no significant difference in Id4 expression levels was found between SS and healthy controls (Fig. 4B). These results indicate that Id4 might be involved in the pathogenesis of IgG4-RD but not SS.

3.5. miR-486-5p is upregulated in IgG4-RD patients, and it regulates Id4 expression in salivary gland cells

We next clarified the mechanism by which Id4 expression was decreased in the salivary glands of IgG4-RD patients. miRNAs are powerful gene regulators that mediate their effects mainly *via* the regulation of mRNA stability and translation, which are involved in most biological processes [18,47]. It was confirmed that Id4 expression levels

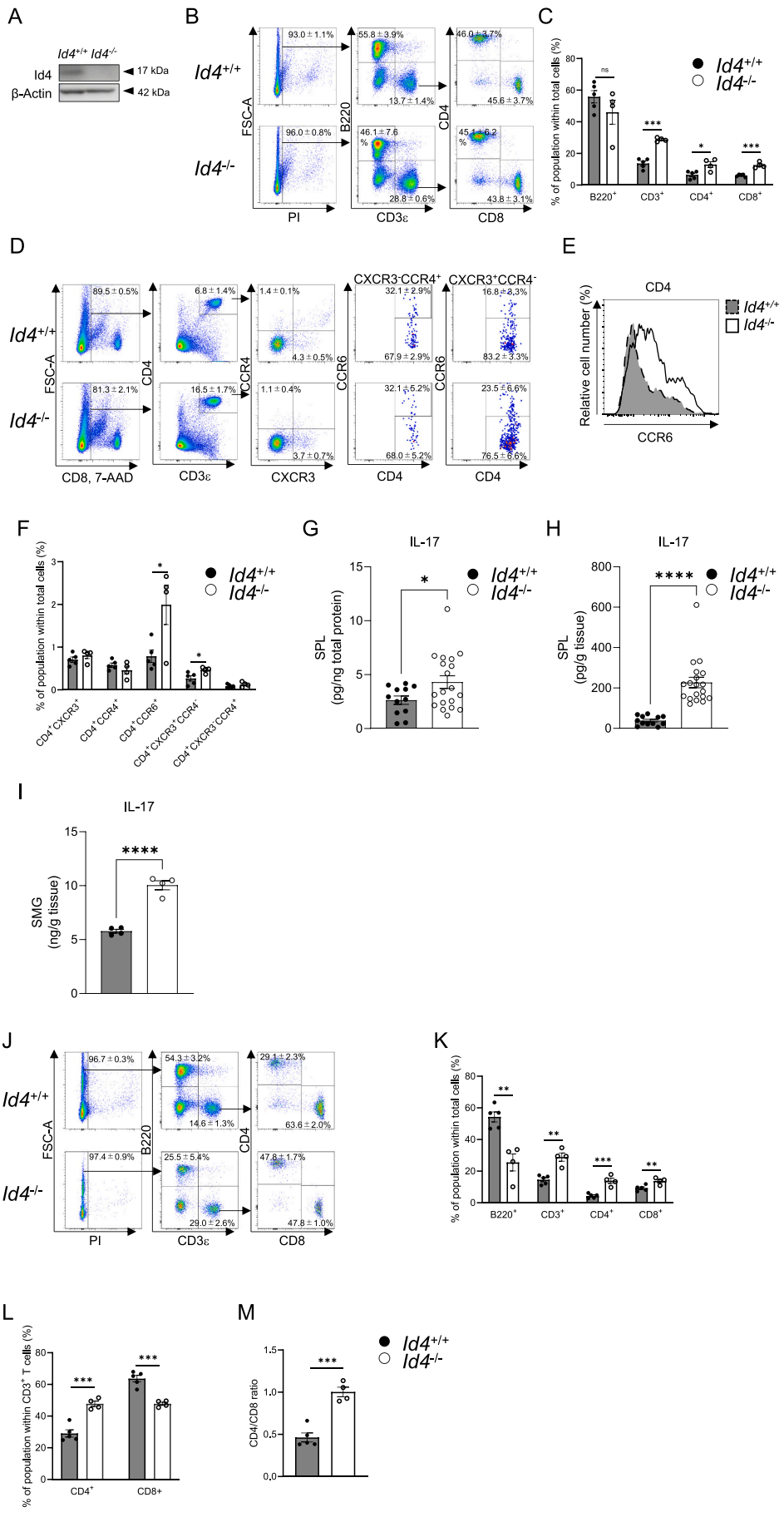

Fig. 3. Id4 deficiency induces the expansion of Th17 cells in the spleen.

(A) Immunoblot analysis of Id4 and β-actin (as a loading control) in the spleens of *Id4*$^{+/+}$ and *Id4*$^{-/-}$ mice. (B–C) FACS plots of splenocytes from *Id4*$^{+/+}$ (upper) and *Id4*$^{-/-}$ mice (lower) (B). The graph represents the frequency of B220^{+} B cells and CD3^{+}, CD4^{+}, and CD8^{+} T cells in the splenocytes (C). (D–F) FACS plots of Th1/Th2/Th17 phenotypes in the splenocytes of *Id4*$^{+/+}$ (upper) and *Id4*$^{-/-}$ mice (lower) (D). Histogram of CCR6 in CD4^{+} T cells in the splenocytes (*Id4*$^{+/+}$, broken line; *Id4*$^{-/-}$, solid line) (E). Graph of the frequency of CD4^{+}CXCR3^{+}, CD4^{+}CCR4^{+}, CD4^{+}CCR6^{+}, CD4^{+}CXCR3^{+}CCR4^{-}, and CD4^{+}CXCR3^{-}CCR4^{+} T cells in the splenocytes of *Id4*$^{+/+}$ and *Id4*$^{-/-}$ mice (F). (G–I) ELISA for IL-17A in splenocytes (G–H) and SMGs (I) from *Id4*$^{+/+}$ and *Id4*$^{-/-}$ mice, using an LBIS Mouse IL-17A ELISA Kit (Fujifilm Wako) (*Id4*$^{+/+}$ $n = 12$; *Id4*$^{-/-}$ $n = 19$ for splenocytes, *Id4*$^{+/+}$ $n = 4$; *Id4*$^{-/-}$ n = 4 for SMGs). The total amount of IL-17A in splenocytes was normalized to the total protein in splenocytes (G) and the spleen tissue weight (H, I). (J–M) FACS plots of PBMCs from *Id4*$^{+/+}$ (upper) and *Id4*$^{-/-}$ mice (lower) (J). Graphs represent the frequency of B220^{+} B cells, CD3^{+}, CD4^{+}, and CD8^{+} T cells in PBMCs (K). The percentages of CD4^{+} and CD8^{+} T cells within CD3^{+} T cells in PBMCs (L), and each calculated CD4^{+}/CD8^{+} ratio in PBMCs (M) by comparing *Id4*$^{+/+}$ and *Id4*$^{-/-}$ mice (*Id4*$^{+/+}$ $n = 5$; *Id4*$^{-/-}$ $n = 4$). All experiments were repeated three times independently, and representative results are shown. A two-tailed Student's *t*-test was used. *$P < 0.05$, **$P < 0.01$, ***$P < 0.001$, ****$P < 0.0001$.

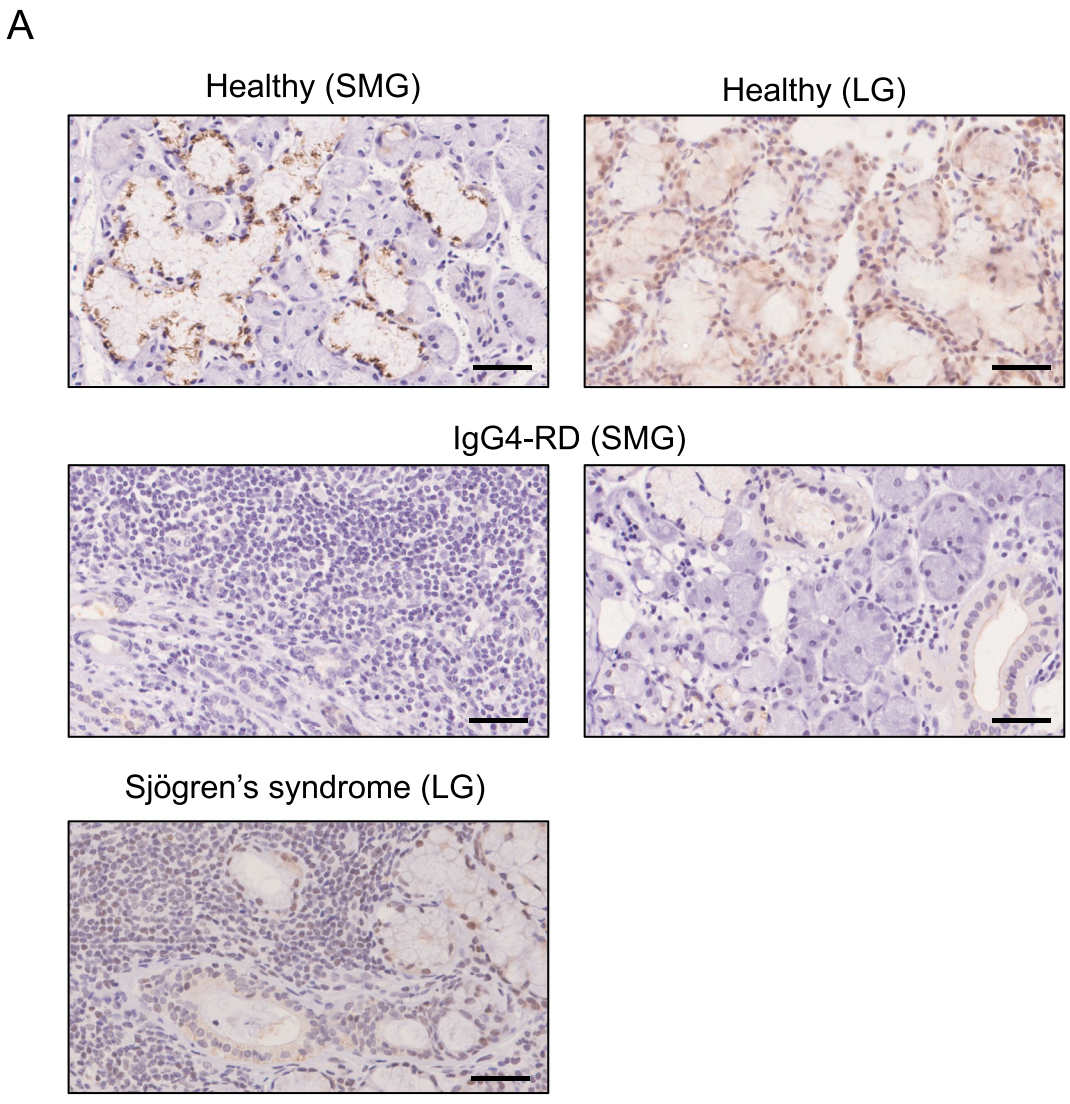

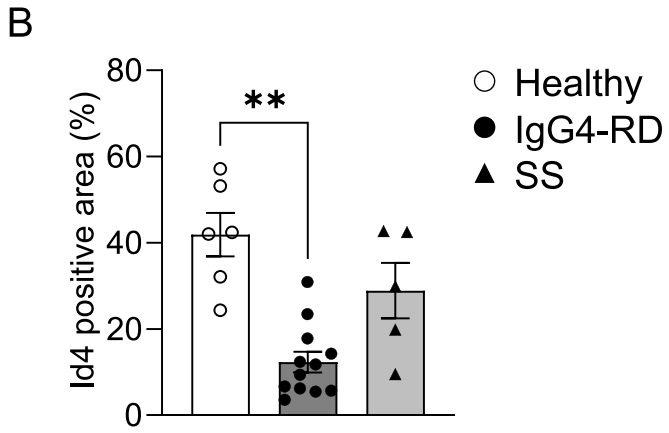

Fig. 4. Id4 expression is markedly reduced in the salivary glands of IgG4-RD patients.
(A–B) Representative images of immunohistochemical staining for Id4 in the SMG (healthy donor) and LG (mucocele) (upper), the SMG from IgG4-RD patients (middle), and the LG from SS patients (lower) (A) and quantitative analysis (B). Scale bars: 50 μm. Salivary glands from healthy donors ($n = 6$), IgG4-RD patients (n

= 12), and SS patients (n = 5) were analyzed. Id4 stained area in nuclei of acinar cell was recognized as Id4 positive area. Data are expressed as the mean ± SE of three independent experiments. Kruskal Wallis test followed by Dunn's multiple comparison test were used. $^{**}P < 0.01$. (C–D) RNAscope *in situ* hybridization against *Id4* expression (brown dots) in salivary glands from healthy donors (left, $n = 3$) and IgG4-RD patients (right, n = 5) (C) and quantitative analysis (D). Scale bar: 100 μm. Magnified images of ISH are indicated in the lower panels. Triangle indicates *Id4* expression. Data are expressed as the mean ± SE of three independent experiments. Welch's *t*-test (two-tailed) was used. $^{**}P < 0.01$.

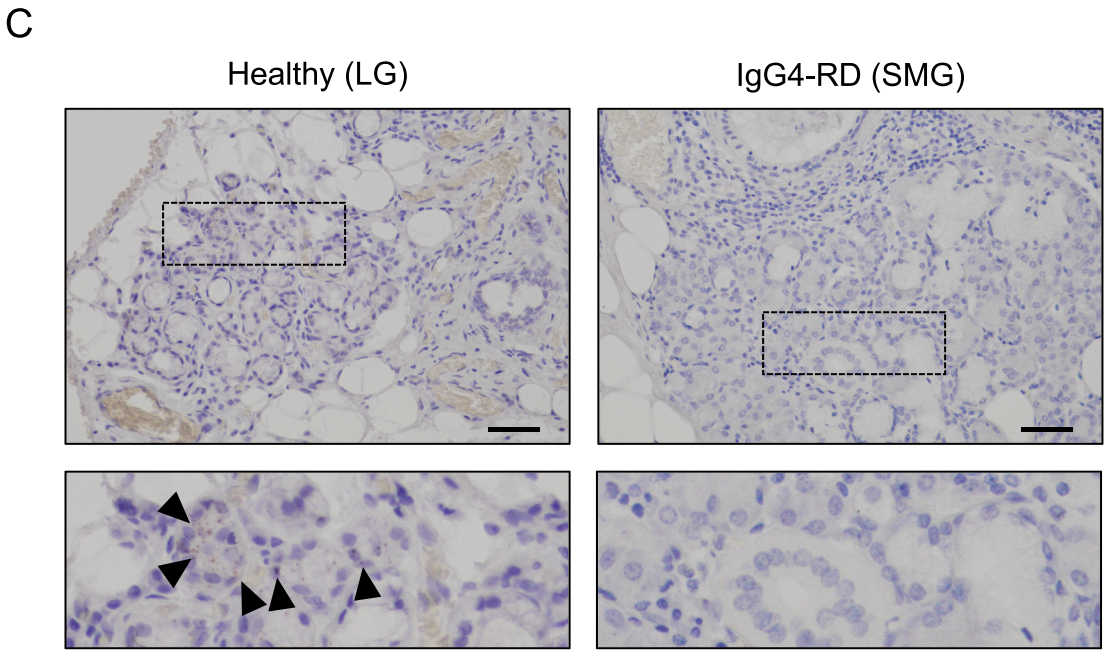

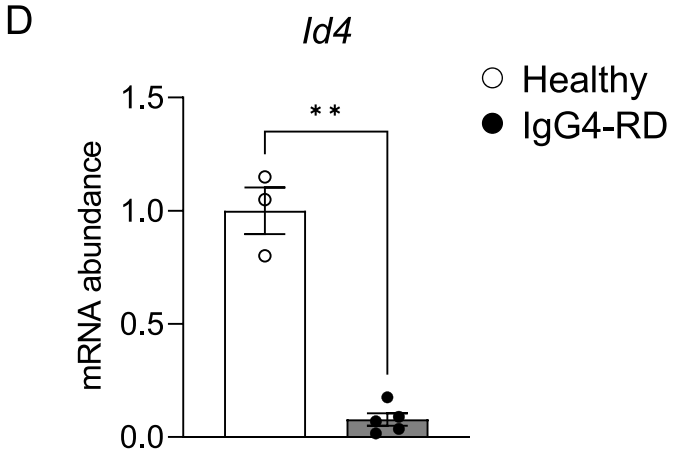

Fig. 4. (*continued*).

were downregulated in the salivary glands of IgG4-RD patients compared to healthy donors, not only at protein levels (Fig. 4A, B) but also mRNA levels (Fig. 4C, D). Therefore, we investigated a potential miRNA-mRNA regulatory axis in IgG4-RD pathogenesis by miRNA-mRNA integrated analysis, using human serum and RSMG-1 cells. A miRNA array using serum from IgG4-RD patients and healthy donors showed that 28 and 31 miRNAs were significantly upregulated or downregulated, respectively, in the serum from IgG4-RD patients compared with healthy controls (Fig. 5A). mRNA changes in RSMG-1 cells that were treated with the same serum samples used for the miRNA array were comprehensively investigated by mRNA array. An *in silico* analysis of each seed sequence of human miRNAs and their complementary sequence of rat mRNAs showed 19 upregulated and 13 downregulated miRNAs, and 60 mRNAs were picked up as candidates (Supplemental Tables 3, 4). Next, we validated the expression levels of these candidate genes in RSMG-1 cells treated with serum from IgG4-RD patients or healthy donors (Fig. 5B, C) using quantitative RT-PCR analysis, and 10 mRNAs, including *Id4*, were selected as candidates.

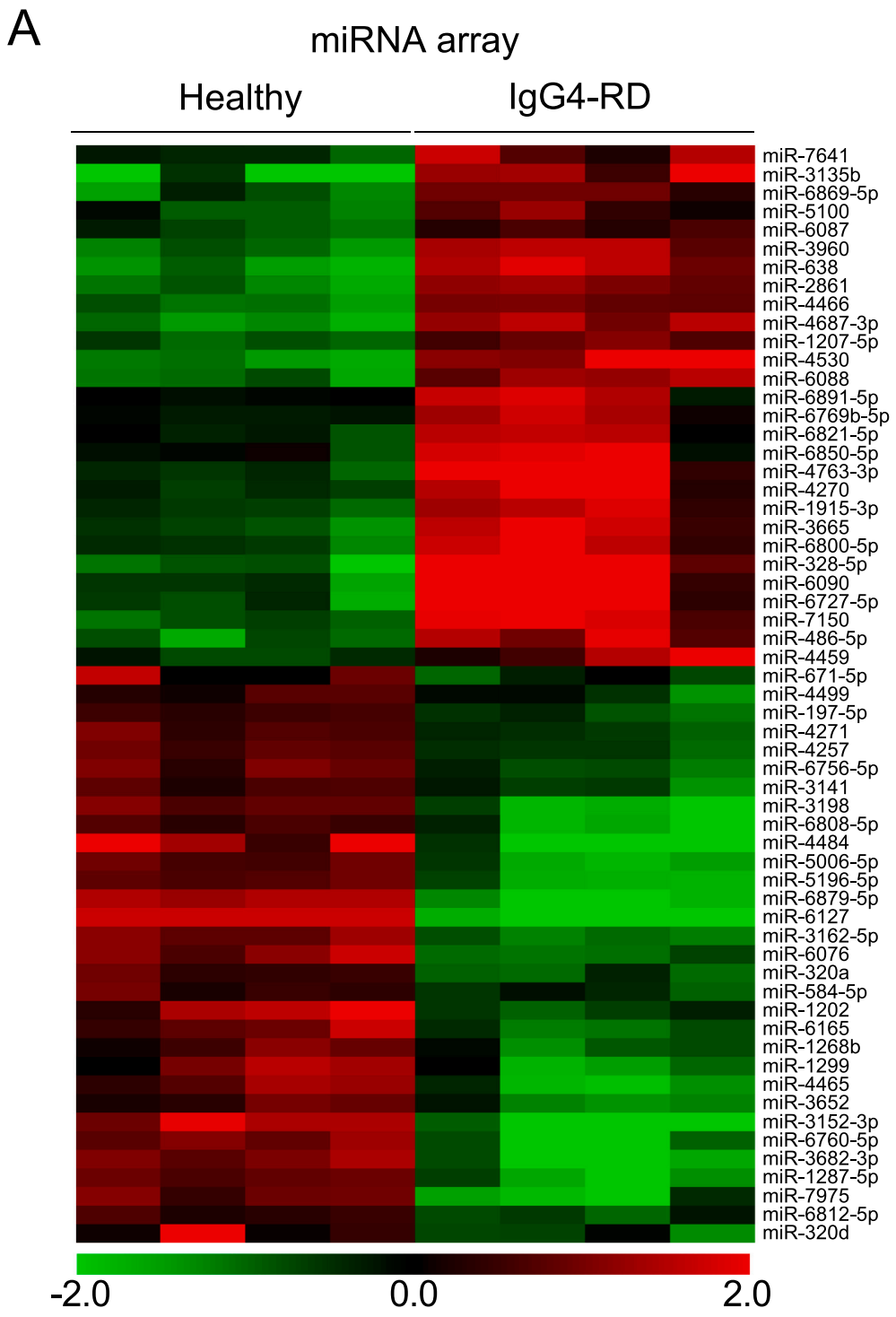

Fig. 5. Id4 expression is suppressed in IgG4-RD *via* the upregulation of miR-486-5p expression.
(A) A heatmap of differentially expressed miRNAs by the miRNA array of serum from IgG4-RD patients compared with healthy donors ($n = 4$, >2-fold change, $p < 0.05$). The color code represents the expression levels of each miRNA as indicated in the lower scale. (B–C) Quantitative RT-PCR analysis of genes that were significantly downregulated (B) or upregulated (C) in RSMG-1 cells after treatment with serum from IgG4-RD patients. (D) Quantitative RT-PCR analysis for *Id4* in PC-3, MCF-7, and Caco-2 cells after treatment with a mimic or inhibitor of miR486-5p. The gene expression of *16S* was determined as the reference gene. (E) The expression levels of miR-486-5p in the serum of healthy donors, IgG4-RD, and SS patients (n = 4). SNORD44 was used as an internal control. Data are expressed as the mean ± SE of three independent experiments. Student's *t*-test (two-tailed) and one-way ANOVA followed by the Tukey-Kramer test were used. $^{*}P < 0.05$, $^{**}P < 0.01$, $^{***}P < 0.001$.

Of these, we collated genes with complementary sequences against the specific miRNA seed sequence that were common in rats and humans using the UCSC Genome Browser database (https://genome.ucsc.edu). We found complementary sequences against the seed sequences of has-miR-3135b, has-miR-3652, and has-miR-486-5p, in the 3′ UTR of *XKR4*, *MAFF*, and *Id4*, respectively (Fig. S2A, B). Previous studies have

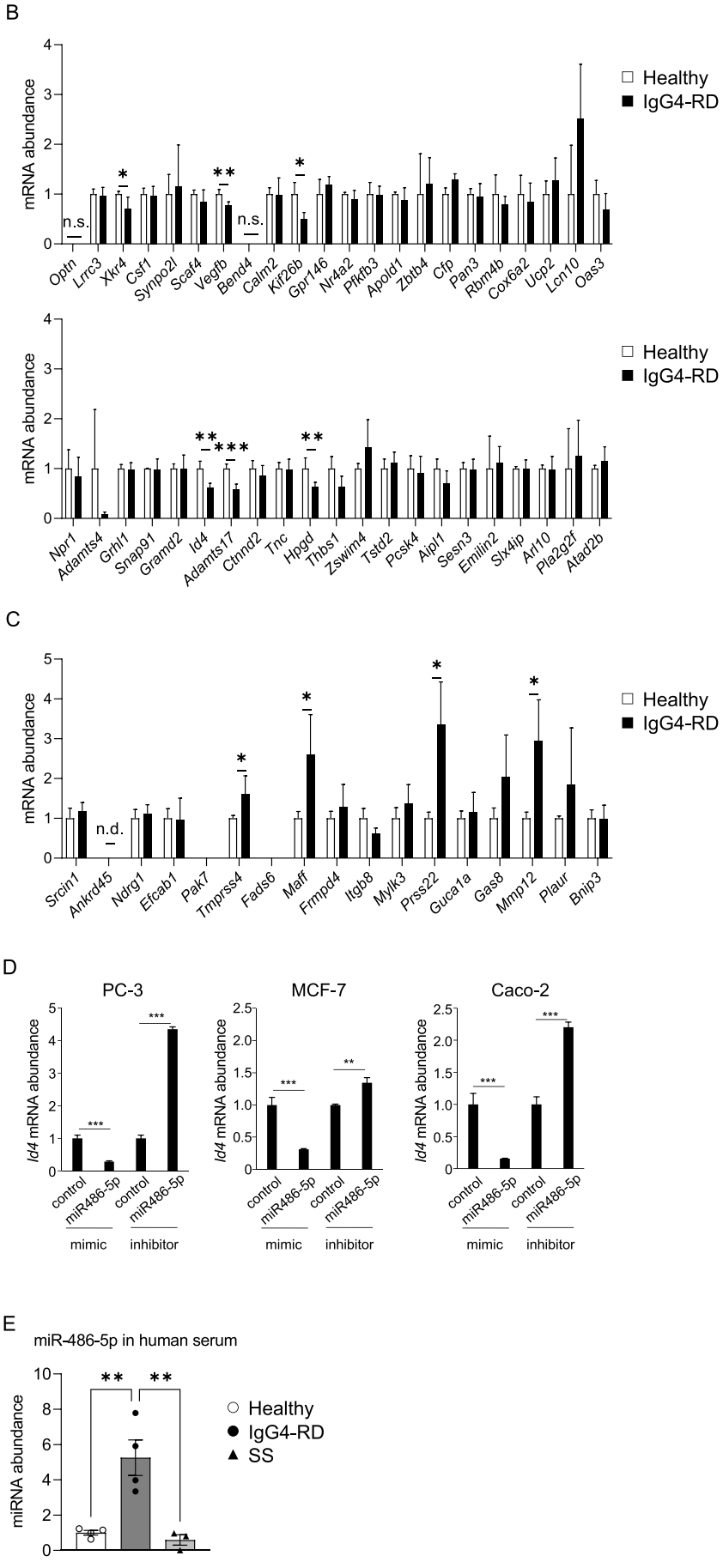

Fig. 5. (*continued*).

reported many common gene targets in miRNA-related cellular pathways across species [48,49]. We thus examined whether these three miRNAs regulated their respective target mRNAs originating from humans, as well as rats, using the human cell lines, PC-3, MCF-7, and Caco-2. A has-miR-486-5p mimic significantly suppressed *Id4* mRNA expression, and its inhibitor increased the expression level of *Id4* mRNA (Fig. 5D). However, has-miR-3135b and has-miR-3652 did not change the expression levels of *XKR4* and *MAFF* mRNAs, respectively, in the human cell lines (data not shown). Indeed, our qPCR analysis demonstrated higher has-miR-486-5p levels in the serum of IgG4-RD patients compared with healthy donors (Fig. 5E). Taken together, these results suggest that the amount of miR486-5p was upregulated under IgG4-RD pathological conditions and accordingly, the expression of *Id4* was suppressed in the salivary glands of these patients.

4. Discussion

This study demonstrated that *Id4* deficiency in mice caused the abnormal differentiation and dysfunction of salivary glands, and increased the proportion of $CD3^+CD4^+CCR6^+$ IL-17-producing Th17 cells, which might be involved in the pathologies of SS or IgG4-RD [41,42,50]. In addition, our study using human samples revealed that Id4 expression was markedly reduced in the lesion sites of IgG4-RD. Furthermore, miRNA-mRNA integrated analysis using human serum demonstrated the regulation of *Id4* mRNA expression by miR-486-5p in normal salivary gland cells, which was the only miRNA-mRNA regulatory network in our analysis. Indeed, serum miR486-5p levels in IgG4-RD patients were significantly increased (Fig. 5E). This result highlights the importance of miR-486-5p and Id4 for salivary gland homeostasis and IgG4-RD pathogenesis.

IgG4-RD is a relatively new fibro-inflammatory disorder that affects multiple organs, in which the infiltration of IgG4-positive plasma cells into various organs and increased IgG4 concentrations in serum are observed [12]. IgG4-RD patients usually develop salivary gland swelling and dry mouth, which are frequently observed in the field of dentistry. It is still unclear what causes the pathogenesis of IgG4-RD, but it might involve the infiltration of high percentages of $IgG4^+$ plasma cells or tissue fibrosis. In addition, most previous studies that focused on the pathological analysis of IgG4-RD used an immunological approach, and few studies have investigated the changes between normal to pathogenic conditions at the lesion site. In this study, we proposed that Id4 might be regulated by hsa-miR-486-5p, a candidate biomarker at the lesion site, which provides valuable new information when investigating the pathophysiology of IgG4-RD.

hsa-miR-486-5p is located on human chromosome 8p 11.21 and might be a biomarker for sarcopenia [51], endometrial cancer [52], chronic myeloid leukemia [53], polycystic ovary syndrome [54], sepsis [55], and inflammatory-related diseases such as osteoarthritis [56]. It is also involved in B cell functions [57] and cellular senescence [58]; however, its relevance in autoimmune diseases is unclear. Napolitano et al. demonstrated that *Id4* is a downstream gene of senescence-related miR-486-5p in human primary fibroblasts [58]. Fibroblast senescence contributes to fibrosis [59], which is a pathological characteristic of IgG4-RD lesions [12]. In addition, Id4 might have an inhibitory effect on the transforming growth factor (TGF)-β signaling pathway [60], which is involved in fibrosis, as well as cell differentiation and proliferation [61].

This study had some limitations. First, we could not use $Id4^{-/-}$ mice at an age corresponding to the age of onset of IgG4-RD because they were subject to premature death. This might explain why we did not observe IgG4-RD-like histological features such as fibrosis and lymphocyte infiltration in the salivary glands of $Id4^{-/-}$ mice. In addition, it might be necessary to further discuss the possibility that Th17 expansion in $Id4^{-/-}$ mice at P21 is truly involved in the pathogenesis process of IgG4-RD, because the significance of Th17 in the pathology of IgG4-RD is controversial [62]. Thus, it will be necessary to verify whether these mice are useful as a model for IgG4-RD by using conditional knockout mice.

Second, IgG4 antibodies have different properties. Because mice lack the IgG4 antibody subtype [63], we were unable to mimic conditions that were completely consistent with the diagnostic criteria for IgG4-RD, although the significance of elevated IgG4 levels in IgG4-RD pathology is controversial [64]. The IgG1 subclass in previously proposed IgG4-RD mouse models, including LATY136-knock-in mice [65] and hu*TLR-7*-transgenic/m$TLR\text{-}7^{-/-}$ mice [66,67] was considered a homolog of human IgG4 [68] because of their functional equivalency. From an immunological aspect, we showed that $Id4^{-/-}$ mice had an increased CD4/CD8 ratio, as well as an increase in Th17 cell numbers (Fig. 3B–M), which are often reported in IgG4-RD, as well as several autoimmune diseases [69–73]. Notably, Th17 cells were significantly increased in IgG4-RD patients compared with healthy controls [41], indicating that Th17 cells might be also related to IgG4-RD, though the exact role of Th17 and IL-17 in the pathogenesis of IgG4-RD has not been clarified yet.

In addition, Id2, an Id protein that suppresses immunoglobulin class switching in mice [74], was also downregulated in the SMG of $Id4^{-/-}$ mice in our study (Fig. S3). These implications raise the possibility that Id4 expression is related to IgG4-RD pathophysiological mechanism.

Third, it is unclear how differentiation abnormalities seen in $Id4^{-/-}$ mice are involved in IgG4-RD. Our supplemental data (Fig. S4) showed the expression of collagen type XVII (COL17A), a hemidesmosome constituent protein, was remarkably reduced in the basal lamina of SMG in IgG4-RD. COL17A has a fundamental role in the regulation of cell proliferation and differentiation [75], and its loss or aberrant expression induces abnormal differentiation [76–78] or neoplasms [79]. On the basis of this evidence, detailed analyses are needed in the future to determine whether abnormal differentiation exists in the background of IgG4-RD pathological conditions.

Last, we used a normal salivary gland cell line from rats in our miRNA-mRNA comprehensive analysis. Because no cell line originating from human normal salivary glands is commercially available, we used RSMG-1 cells in our analysis because we considered it important to analyze the pathological process from a normal status in salivary glands. Therefore, other miRNAs, except hsa-miR-486-5p, and their downstream mRNAs might be involved in the pathogenesis of IgG4-RD. In this study, human, rat, and mouse *Id4* mRNAs had the same complementary sequence for the seed sequence of miR-486-5p; therefore, we investigated the association between miR-486-5p and *Id4* mRNA in the pathogenesis of IgG4-RD.

Of the Id proteins (Id1–Id3) [1], Id3 mimics the phenotype of SS [80], and induces the expansion of Th17 cells [81]. In addition, Id1 [82] and Id2 [83] are associated with autoimmune reactions, whereas Id4 has not been suggested to have direct relevance to immune-related diseases. Id proteins perform their biological functions *via* protein-protein interactions, some of which are specific to individual Id proteins. Supplemental Fig. 3 shows the expression levels of Id family genes in the SMG of $Id4^{-/-}$ mice to confirm whether Id4 deficiency affected the expressions of other Id molecules related to compensatory effects. For unknown reasons, the expression levels of Id1 and Id3 were increased, whereas those of Id2 were decreased in the SMG of $Id4^{-/-}$ mice (Fig. S3). It is unclear whether these expressional fluctuations caused by *Id4* deficiency affected the pathological conditions of $Id4^{-/-}$ mice. However, this supports the finding that $Id4^{-/-}$ mice survive under an abnormal immune system until the end of their short lives. For example, considering that Id1, Id2, and Id3 have each important role on the regulation of immune balance [84], this expression fluctuation might be one of the reasons why impaired balance of CD4/CD8 ratio in $Id4^{-/-}$ mice. In summary, our study indicated that Id4 regulates normal salivary gland differentiation and its decreased expression leads to disruption of salivary gland homeostasis. Future studies should help us to understand the role of hsa-miR-486-5p and Id4 in the pathogenesis of IgG4-RD.

CRediT authorship contribution statement

Y.H., S.K., S.Y., and T.K-Y. designed and performed experiments, analyzed data, and wrote the manuscript. E.Y., and S.Y. performed experiments and analyzed data. A.S., A.Y., J.K., Y.H., M.M., S.N., and E.J. provided suggestions for experiments and data analysis, evaluated the data, and participated in preparing the manuscript.

Declaration of competing interest

The authors declare that they have no known competing financial interests or personal relationships that could have appeared to influence the work reported in this paper.

Data availability

Data will be made available on request.

Acknowledgements

The authors thank Hikari Takeshima, Mayu Seida, and Nao Kuboyama for helpful technical assistance; Dr. Mizuki Sakamoto for the data sorting of human samples; Dr. Atsushi Doi, Dr. Hiroko Hagiwara, and Dr. Kaori Yasuda (Cell Innovator, Fukuoka, Japan) for assistance with the miRNA and mRNA array analyses and useful discussions. We appreciate the technical assistance of the Research Support Center, Research Center for Human Disease Modeling, Kyushu University Graduate School of Medical Sciences. We thank J. Ludovic Croxford, PhD, from Edanz (https://jp.edanz.com/ac) for editing a draft of this manuscript.

Funding

This study was supported by the Japan Society for the Promotion of Science (KAKENHI grants JP20K17381 to Y.H., JP20K23114 and JP22K17003 to E.Y., JP19K10052 and JP22K09914 to T.K.-Y., JP19K10269 and JP22K10173 to A.Y., and JP20H00553 to S.N.), Takeda Science Foundation (S.Y. and T.K.-Y.), Kaibara Morikazu Medical Science Promotion Foundation (S.Y.), Fukuoka Public Health Promotion Organization Cancer Research Fund (S.Y.), Kakihara Science Technology Foundation (T.K.-Y.), Kenko Kagaku Zaidan (T.K.-Y.), Astellas Foundation for Research on Metabolic Disorders (T.K.-Y.), and Mishima Kaiun Memorial Foundation (T.K.-Y.).

Appendix A. Supplementary data

Supplementary data to this article can be found online at https://doi.org/10.1016/j.bbamcr.2022.119404.

References

[1] R. Benezra, R.L. Davis, D. Lockshon, D.L. Turner, H. Weintraub, The protein id: a negative regulator of helix-loop-helix DNA binding proteins, Cell 61 (1990) 49–59.
[2] H.A. Sikder, M.K. Devlin, S. Dunlap, B. Ryu, R.M. Alani, Id proteins in cell growth and tumorigenesis, Cancer Cell 3 (2003) 525–530.
[3] J. Ke, R. Wu, Y. Chen, M.L. Abba, Inhibitor of DNA binding proteins: implications in human cancer progression and metastasis, Am. J. Transl. Res. 10 (2018) 3887–3910.
[4] L.H. Wang, N.E. Baker, E. Proteins, I.D. Proteins, Helix-loop-helix partners in development and disease, Dev. Cell 35 (2015) 269–280.
[5] V. Riechmann, I. van Crüchten, F. Sablitzky, The expression pattern of Id4, a novel dominant negative helix-loop-helix protein, is distinct from Id1, Id2 and Id3, Nucleic Acids Res. 22 (1994) 749–755.
[6] Y. Jen, K. Manova, R. Benezra, Expression patterns of Id1, Id2, and Id3 are highly related but distinct from that of Id4 during mouse embryogenesis, Dev. Dyn. 207 (1996) 235–252.
[7] F. Sablitzky, A. Moore, M. Bromley, R.W. Deed, J.S. Newton, J.D. Norton, Stage- and subcellular-specific expression of Id proteins in male germ and Sertoli cells implicates distinctive regulatory roles for Id proteins during meiosis, spermatogenesis, and Sertoli cell function, Cell Growth Differ. 9 (1998) 1015–1024.
[8] S.A. Best, K.J. Hutt, N.Y. Fu, F. Vaillant, S.H. Liew, L. Hartley, C.L. Scott, G. J. Lindeman, J.E. Visvader, Dual roles for Id4 in the regulation of estrogen signaling in the mammary gland and ovary, Development 141 (2014) 3159–3164.
[9] H. Holliday, D. Roden, S. Junankar, S.Z. Wu, L.A. Baker, C. Krisp, C.L. Chan, A. McFarland, J.N. Skhinas, T.R. Cox, B. Pal, N.D. Huntington, C.J. Ormandy, J. S. Carroll, J. Visvader, M.P. Molloy, A. Swarbrick, Inhibitor of Differentiation 4 (ID4) represses mammary myoepithelial differentiation via inhibition of HEB, iScience 24 (2021) 102072.
[10] Y. Tokuzawa, K. Yagi, Y. Yamashita, Y. Nakachi, I. Nikaido, H. Bono, Y. Ninomiya, Y. Kanesaki-Yatsuka, M. Akita, H. Motegi, S. Wakana, T. Noda, F. Sablitzky, S. Arai, R. Kurokawa, T. Fukuda, T. Katagiri, C. Schönbach, T. Suda, Y. Mizuno, Y. Okazaki, Id4, a new candidate gene for senile osteoporosis, acts as a molecular switch promoting osteoblast differentiation, PLoS Genet. 6 (2010), e1001019.
[11] W. Chen, Y. Yu, J. Ma, N. Olsen, J. Lin, Mesenchymal stem cells in primary Sjögren's syndrome: prospective and challenges, Stem Cells Int. 2018 (2018) 4357865.
[12] F. Peyronel, A. Vaglio, F. Maritati, IgG4-related disease: a clinical perspective, Rheumatology (Oxford, England) 59 (2020) iii123–iii131.
[13] J. Tang, S. Cai, C. Ye, L. Dong, Biomarkers in IgG4-related disease: a systematic review, Semin. Arthritis Rheum. 50 (2020) 354–359.
[14] G.E. Fragoulis, E. Zampeli, H.M. Moutsopoulos, IgG4-related sialadenitis and Sjögren's syndrome, Oral Dis. 23 (2017) 152–156.
[15] M. Lanzillotta, G. Mancuso, E. Della-Torre, Advances in the diagnosis and management of IgG4 related disease, BMJ (Clin. Res. Ed.) 369 (2020), m1067.
[16] N. Nezu, Y. Usui, M. Asakage, H. Shimizu, K. Tsubota, A. Narimatsu, K. Umazume, N. Yamakawa, S.I. Ohno, M. Takanashi, M. Kuroda, H. Goto, Distinctive tissue and serum MicroRNA profile of IgG4-related ophthalmic disease and MALT lymphoma, J. Clin. Med. 9 (2020).
[17] B.P. Lewis, I.H. Shih, M.W. Jones-Rhoades, D.P. Bartel, C.B. Burge, Prediction of mammalian microRNA targets, Cell 115 (2003) 787–798.
[18] M. Ha, V.N. Kim, Regulation of microRNA biogenesis, Nat. Rev. Mol. Cell Biol. 15 (2014) 509–524.
[19] M. Furue, T. Okamoto, H. Hayashi, J.D. Sato, M. Asashima, S. Saito, Effects of hepatocyte growth factor (HGF) and activin A on the morphogenesis of rat submandibular gland-derived epithelial cells in serum-free collagen gel culture, in vitro cellular & developmental biology, Animal 35 (1999) 131–135.
[20] L. Bedford, R. Walker, T. Kondo, I. van Crüchten, E.R. King, F. Sablitzky, Id4 is required for the correct timing of neural differentiation, Dev. Biol. 280 (2005) 386–395.
[21] M.P. Hoffman, B.L. Kidder, Z.L. Steinberg, S. Lakhani, S. Ho, H.K. Kleinman, M. Larsen, Gene expression profiles of mouse submandibular gland development: FGFR1 regulates branching morphogenesis in vitro through BMP- and FGF-dependent mechanisms, Development (Cambridge, England) 129 (2002) 5767–5778.
[22] B.P. Lewis, C.B. Burge, D.P. Bartel, Conserved seed pairing, often flanked by adenosines, indicates that thousands of human genes are microRNA targets, Cell 120 (2005) 15–20.
[23] A. Grimson, K.K. Farh, W.K. Johnston, P. Garrett-Engele, L.P. Lim, D.P. Bartel, MicroRNA targeting specificity in mammals: determinants beyond seed pairing, Mol. Cell 27 (2007) 91–105.
[24] C.H. Chou, N.W. Chang, S. Shrestha, S.D. Hsu, Y.L. Lin, W.H. Lee, C.D. Yang, H. C. Hong, T.Y. Wei, S.J. Tu, T.R. Tsai, S.Y. Ho, T.Y. Jian, H.Y. Wu, P.R. Chen, N. C. Lin, H.T. Huang, T.L. Yang, C.Y. Pai, C.S. Tai, W.L. Chen, C.Y. Huang, C.C. Liu, S. L. Weng, K.W. Liao, W.L. Hsu, H.D. Huang, miRTarBase 2016: updates to the experimentally validated miRNA-target interactions database, Nucleic Acids Research 44 (2016) D239–D247.
[25] E. Berezikov, V. Guryev, J. van de Belt, E. Wienholds, R.H.A. Plasterk, E. Cuppen, Phylogenetic Shadowing and Computational Identification of Human microRNA Genes, Cell 120 (2005) 21–24.
[26] M. Furue, Y. Zhang, T. Okamoto, R.I. Hata, M. Asashima, Activin A induces expression of rat Sel-1l mRNA, a negative regulator of notch signaling, in rat salivary gland-derived epithelial cells, Biochem. Biophys. Res. Commun. 282 (2001) 745–749.
[27] H.S. Larsen, M.H. Aure, S.B. Peters, M. Larsen, E.B. Messelt, H. Kanli Galtung, Localization of AQP5 during development of the mouse submandibular salivary gland, J. Mol. Histol. 42 (2011) 71–81.
[28] A.J. May, N. Cruz-Pacheco, E. Emmerson, E.A. Gaylord, K. Seidel, S. Nathan, M. O. Muench, O.D. Klein, S.M. Knox, Diverse progenitor cells preserve salivary gland ductal architecture after radiation-induced damage, Development (Cambridge, England) 145 (2018).
[29] A. Kuony, F. Michon, Epithelial markers aSMA, Krt14, and Krt19 unveil elements of murine lacrimal gland morphogenesis and maturation, Front. Physiol. 8 (2017) 739.
[30] P.R. Clarke, L.A. Allan, Cell-cycle control in the face of damage–a matter of life or death, Trends Cell Biol. 19 (2009) 89–98.
[31] C. Rocchi, L. Barazzuol, R.P. Coppes, The evolving definition of salivary gland stem cells, NPJ Regen. Med. 6 (2021) 4.
[32] A.M.L. Pedersen, C.E. Sørensen, G.B. Proctor, G.H. Carpenter, J. Ekström, Salivary secretion in health and disease, J. Oral Rehabil. 45 (2018) 730–746.
[33] A.J. May, L. Chatzeli, G.B. Proctor, A.S. Tucker, Salivary gland dysplasia in Fgf10 heterozygous mice: a new mouse model of xerostomia, Curr. Mol. Med. 15 (2015) 674–682.

[34] H. Tsuboi, F. Honda, H. Takahashi, Y. Ono, S. Abe, Y. Kondo, I. Matsumoto, T. Sumida, Pathogenesis of IgG4-related disease. Comparison with Sjögren's syndrome, Modern Rheumatology 30 (2020) 7–16.
[35] R.I. Fox, Sjögren's syndrome, Lancet (London, England) 366 (2005) 321–331.
[36] J. Borst, T. Ahrends, N. Bąbała, C.J.M. Melief, W. Kastenmüller, CD4(+) T cell help in cancer immunology and immunotherapy, Nat. Rev. Immunol. 18 (2018) 635–647.
[37] S.M. Paulissen, J.P. van Hamburg, W. Dankers, E. Lubberts, The role and modulation of CCR6+ Th17 cell populations in rheumatoid arthritis, Cytokine 74 (2015) 43–53.
[38] A. Singhania, P. Dubelko, R. Kuan, W.D. Chronister, K. Muskat, J. Das, E.J. Phillips, S.A. Mallal, G. Seumois, P. Vijayanand, A. Sette, M. Lerm, B. Peters, C. Lindestam Arlehamn, CD4+CCR6+ T cells dominate the BCG-induced transcriptional signature, EBioMedicine 74 (2021) 103746.
[39] H. Bai, J. Cheng, X. Gao, A.G. Joyee, Y. Fan, S. Wang, L. Jiao, Z. Yao, X. Yang, IL-17/Th17 promotes type 1 T cell immunity against pulmonary intracellular bacterial infection through modulating dendritic cell function, J. Immunol. (Baltimore, Md.: 1950) 183 (2009) 5886–5895.
[40] K.E. Marks, D.A. Rao, T peripheral helper cells in autoimmune diseases, Immunol. Rev. 307 (2022) 191–202.
[41] A. Grados, M. Ebbo, C. Piperoglou, M. Groh, A. Regent, M. Samson, B. Terrier, A. Loundou, N. Morel, S. Audia, F. Maurier, J. Graveleau, M. Hamidou, A. Forestier, S. Palat, E. Bernit, B. Bonotte, C. Farnarier, J.R. Harlé, N. Costedoat-Chalumeau, F. Vély, N. Schleinitz, T cell polarization toward T(H)2/T(FH)2 and T(H)17/T(FH)17 in patients with IgG4-related disease, Front. Immunol. 8 (2017) 235.
[42] G.M. Verstappen, O.B.J. Corneth, H. Bootsma, F.G.M. Kroese, Th17 cells in primary Sjögren's syndrome: pathogenicity and plasticity, J. Autoimmun. 87 (2018) 16–25.
[43] N. Singh, P.L. Cohen, The T cell in Sjogren's syndrome: force majeure, not spectateur, J. Autoimmun. 39 (2012) 229–233.
[44] H. Mattoo, J.H. Stone, S. Pillai, Clonally expanded cytotoxic CD4(+) T cells and the pathogenesis of IgG4-related disease, Autoimmunity 50 (2017) 19–24.
[45] K. Błochowiak, P. Celichowski, B. Kempisty, K. Iwanik, M. Nowicki, Transcriptomic profile of genes encoding proteins involved in pathogenesis of Sjögren's syndrome related xerostomia—molecular and clinical trial, J. Clin. Med. 9 (2020) 3299.
[46] T. Maehara, M. Moriyama, H. Nakashima, K. Miyake, J.N. Hayashida, A. Tanaka, S. Shinozaki, Y. Kubo, S. Nakamura, Interleukin-21 contributes to germinal centre formation and immunoglobulin G4 production in IgG4-related dacryoadenitis and sialoadenitis, so-called Mikulicz's disease, Ann. Rheum. Dis. 71 (2012) 2011–2019.
[47] J. O'Brien, H. Hayder, Y. Zayed, C. Peng, Overview of MicroRNA biogenesis, mechanisms of actions, and circulation, Front. Endocrinol. 9 (2018) 402.
[48] I. Güller, S. McNaughton, T. Crowley, V. Gilsanz, S. Kajimura, M. Watt, A. P. Russell, Comparative analysis of microRNA expression in mouse and human brown adipose tissue, BMC Genomics 16 (2015) 820.
[49] H.A. Weisz, D. Kennedy, S. Widen, H. Spratt, S.L. Sell, C. Bailey, M. Sheffield-Moore, D.S. DeWitt, D.S. Prough, H. Levin, C. Robertson, H.L. Hellmich, MicroRNA sequencing of rat hippocampus and human biofluids identifies acute, chronic, focal and diffuse traumatic brain injuries, Sci. Rep. 10 (2020) 3341.
[50] R. Bechara, M.J. McGeachy, S.L. Gaffen, The metabolism-modulating activity of IL-17 signaling in health and disease, J. Exp. Med. 218 (2021).
[51] H.C. Liu, D.S. Han, C.C. Hsu, J.S. Wang, Circulating microRNA-486 and microRNA-146a serve as potential biomarkers of sarcopenia in the older adults, BMC Geriatr. 21 (2021) 86.
[52] X. Zheng, K. Xu, L. Zhu, M. Mao, F. Zhang, L. Cui, MiR-486-5p act as a biomarker in endometrial carcinoma: promotes cell proliferation, migration, invasion by targeting MARK1, OncoTargets Ther. 13 (2020) 4843–4853.
[53] A. Ninawe, S.A. Guru, P. Yadav, M. Masroor, A. Samadhiya, N. Bhutani, N. Gupta, R. Gupta, A. Saxena, miR-486-5p: a prognostic biomarker for chronic myeloid leukemia, ACS Omega 6 (2021) 7711–7718.
[54] F. Cirillo, C. Catellani, P. Lazzeroni, C. Sartori, A. Nicoli, S. Amarri, G.B. La Sala, M. E. Street, MiRNAs regulating insulin sensitivity are dysregulated in polycystic ovary syndrome (PCOS) ovaries and are associated with markers of inflammation and insulin sensitivity, Front. Endocrinol. 10 (2019) 879.
[55] B. Sun, S. Guo, miR-486-5p serves as a diagnostic biomarker for sepsis and its predictive value for clinical outcomes, J. Inflamm. Res. 14 (2021) 3687–3695.
[56] J. Shi, K. Guo, S. Su, J. Li, C. Li, miR-486-5p is upregulated in osteoarthritis and inhibits chondrocyte proliferation and migration by suppressing SMAD2, Mol. Med. Rep. 18 (2018) 502–508.
[57] Z.W. Zhang, M. Wang, J.J. Hu, G. Xu, Y. Zhang, N. Zhang, Decreased expression of microRNA-107 in B lymphocytes of patients with antibody-mediated renal allograft rejection, Tohoku J. Exp. Med. 246 (2018) 87–96.
[58] M. Napolitano, M. Comegna, M. Succoio, E. Leggiero, L. Pastore, R. Faraonio, F. Cimino, F. Passaro, Comparative analysis of gene expression data reveals novel targets of senescence-associated microRNAs, PLoS One 9 (2014), e98669.
[59] A. Usategui, C. Municio, E.G. Arias-Salgado, M. Martín, B. Fernández-Varas, M. J. Del Rey, P. Carreira, A. González, G. Criado, R. Perona, J.L. Pablos, Evidence of telomere attrition and a potential role for DNA damage in systemic sclerosis, Immun. Ageing 19 (2022) 7.
[60] X. Wang, Q. Lu, X. Fei, Y. Zhao, B. Shi, C. Li, H. Chen, Expression and prognostic value of Id-4 in patients with esophageal squamous cell carcinoma, OncoTargets Ther. 13 (2020) 1225–1234.
[61] N.C. Henderson, F. Rieder, T.A. Wynn, Fibrosis: from mechanisms to medicines, Nature 587 (2020) 555–566.
[62] J. Liu, W. Yin, L.S. Westerberg, P. Lee, Q. Gong, Y. Chen, L. Dong, C. Liu, Immune dysregulation in IgG(4)-related disease, Front. Immunol. 12 (2021), 738540.
[63] K. Kamata, T. Watanabe, K. Minaga, W. Strober, M. Kudo, Autoimmune pancreatitis mouse model, Curr. Protoc. Immunol. 120 (2018), 15.31.11–15.31.18.
[64] E. Peuraharju, J. Hagström, J. Tarkkanen, C. Haglund, T. Atula, IgG4-positive plasma cells in nonspecific sialadenitis and sialolithiasis, Mod. Pathol. 35 (2022) 1423–1430.
[65] K. Yamada, M. Zuka, K. Ito, K. Mizuguchi, Y. Kakuchi, T. Onoe, Y. Suzuki, M. Yamagishi, S. Izui, M. Malissen, B. Malissen, M. Kawano, LatY136F knock-in mouse model for human IgG4-related disease, PLoS One 13 (2018), e0198417.
[66] N. Ishiguro, M. Moriyama, K. Furusho, S. Furukawa, T. Shibata, Y. Murakami, A. Chinju, A. Haque, Y. Gion, M. Ohta, T. Maehara, A. Tanaka, M. Yamauchi, M. Sakamoto, K. Mochizuki, Y. Ono, J.N. Hayashida, Y. Sato, T. Kiyoshima, H. Yamamoto, K. Miyake, S. Nakamura, Activated M2 macrophages contribute to the pathogenesis of IgG4-related disease via Toll-like receptor 7/interleukin-33 signaling, Arthritis Rheumatology (Hoboken, N.J.) 72 (2020) 166–178.
[67] A. Chinju, M. Moriyama, N. Kakizoe-Ishiguro, H. Chen, Y. Miyahara, A. Haque, K. Furusho, M. Sakamoto, K. Kai, K. Kibe, S. Hatakeyama-Furukawa, M. Ito-Ohta, T. Maehara, S. Nakamura, CD163+ M2 Macrophages Promote Fibrosis in IgG4-Related Disease Via Toll-like Receptor 7/Interleukin-1 Receptor-Associated Kinase 4/NF-κB Signaling, Arthritis & rheumatology (Hoboken, N.J.) 74 (2022) 892–901.
[68] J. Mestas, C.C. Hughes, Of mice and not men: differences between mouse and human immunology, J. Immunol. 172 (2004) 2731–2738.
[69] B. Charlton, K.J. Lafferty, The Th1/Th2 balance in autoimmunity, Curr. Opin. Immunol. 7 (1995) 793–798.
[70] M.P. Pender, CD8+ T-cell deficiency, Epstein-Barr virus infection, vitamin D deficiency, and steps to autoimmunity: a unifying hypothesis, Autoimmun. Diseases 2012 (2012) 189096.
[71] B.R. Nielsen, R. Ratzer, L. Börnsen, M.R. von Essen, J.R. Christensen, F. Sellebjerg, Characterization of naïve, memory and effector T cells in progressive multiple sclerosis, J. Neuroimmunol. 310 (2017) 17–25.
[72] I. Raphael, R.R. Joern, T.G. Forsthuber, Memory CD4(+) T cells in immunity and autoimmune diseases, Cells 9 (2020).
[73] K.E. Marks, D.A. Rao, T peripheral helper cells in autoimmune diseases, Immunol. Rev. 307 (2022) 191–202.
[74] M. Sugai, H. Gonda, T. Kusunoki, T. Katakai, Y. Yokota, A. Shimizu, Essential role of Id2 in negative regulation of IgE class switching, Nat. Immunol. 4 (2003) 25–30.
[75] J. Tuusa, N. Kokkonen, K. Tasanen, BP180/collagen XVII: a molecular view, Int. J. Mol. Sci. 22 (2021).
[76] N. Liu, H. Matsumura, T. Kato, S. Ichinose, A. Takada, T. Namiki, K. Asakawa, H. Morinaga, Y. Mohri, A. De Arcangelis, E. Geroges-Labouesse, D. Nanba, E. K. Nishimura, Stem cell competition orchestrates skin homeostasis and ageing, Nature 568 (2019) 344–350.
[77] H. Matsumura, Y. Mohri, N.T. Binh, H. Morinaga, M. Fukuda, M. Ito, S. Kurata, J. Hoeijmakers, E.K. Nishimura, Hair follicle aging is driven by transepidermal elimination of stem cells via COL17A1 proteolysis, Science 351 (2016), aad4395.
[78] T. Asaka, M. Akiyama, T. Domon, W. Nishie, K. Natsuga, Y. Fujita, R. Abe, Y. Kitagawa, H. Shimizu, Type XVII collagen is a key player in tooth enamel formation, Am. J. Pathol. 174 (2009) 91–100.
[79] A. Yasukochi, T. Kawakubo-Yasukochi, M. Morioka, M. Hazekawa, T. Nishinakagawa, K. Ono, M. Nakashima, S. Nakamura, Regulation of collagen type XVII expression by miR203a-3p in oral squamous cell carcinoma cells, J. Biochem. 166 (2019) 163–173.
[80] H. Li, M. Dai, Y. Zhuang, A T cell intrinsic role of Id3 in a mouse model for primary Sjogren's syndrome, Immunity 21 (2004) 551–560.
[81] T. Maruyama, J. Li, J.P. Vaque, J.E. Konkel, W. Wang, B. Zhang, P. Zhang, B. F. Zamarron, D. Yu, Y. Wu, Y. Zhuang, J.S. Gutkind, W. Chen, Control of the differentiation of regulatory T cells and T(H)17 cells by the DNA-binding inhibitor Id3, Nat. Immunol. 12 (2011) 86–95.
[82] C. Liu, H.C. Wang, S. Yu, R. Jin, H. Tang, Y.F. Liu, Q. Ge, X.H. Sun, Y. Zhang, Id1 expression promotes T regulatory cell differentiation by facilitating TCR costimulation, J. Immunol. 193 (2014) 663–672.
[83] Y.Y. Lin, M.E. Jones-Mason, M. Inoue, A. Lasorella, A. Iavarone, Q.J. Li, M. L. Shinohara, Y. Zhuang, Transcriptional regulator Id2 is required for the CD4 T cell immune response in the development of experimental autoimmune encephalomyelitis, J. Immunol. 189 (2012) 1400–1405.
[84] A. Pankow, X.H. Sun, The divergence between T cell and innate lymphoid cell fates controlled by E and Id proteins, Front. Immunol. 13 (2022), 960444.